Original Paper

Eletrônica de Potência
Open Journal of Power Electronics

Received March 10, 2025; accepted July 01, 2025; Date of publication July 30, 2025.
The review of this paper was arranged by Associate Editor Filipe P. Scalcon and Editor-in-Chief Heverton A. Pereira.

Digital Object Identifier http://doi.org/10.18618/REP.e202542

Exact Solution of the Class-E Inverter for Wireless Power Transfer Systems

Bruna C. Nicoletti[1], **Fábio E. Bisogno**[2], **Lucas S. Mendonça**[1]

[1]Federal University of Technology – Paraná, Academic Department of Electronics, Curitiba, PR, Brazil.
[2]Hochschule Koblenz, Lehrgebiet Elektronik, Koblenz, Germany.

e-mail: brunanicoletti@alunos.utfpr.edu.br; fbisogno@gmail.com; lucasmendonca@utfpr.edu.br

ABSTRACT This paper introduces the exact solution of the Class-E WPT resonant inverter. Dominantly, the DC-AC inverters for WPT systems are analyzed by assuming a sinusoid waveform for the output variables. However, by allowing waveform light distortions, the magnetic element values can be reduced; which is provided by the proposed method. It is shown that the circuit waveforms are composed of sine, cosine and exponential terms. The obtained solutions are used to design a $500\,\text{kHz}$ Class-E WPT resonant inverter which operates with ZVS. The design is experimentally verified and $74\,\%$ efficiency with $9.7\,\text{W}$ output power is achieved.

KEYWORDS dc-ac inverters, resonant converters, wireless power transfer

I. INTRODUCTION

By means of a variable magnetic field, energy can be wireless transferred, which avoids physical contact between transmitter and receiver devices. This concept is known as inductive wireless power transfer (WPT) and its applications are related to electric vehicle chargers [1]–[3], smart grids [4], portable electronics [5]–[7] and biomedical [8].

In order to drive the transmitter coil, a high-frequency inverter is commonly used, which provides the alternating current injection in the primary side. Several topologies have been studied as DC-AC inverter for the WPT system. Generally, resonant inverters are chosen to drive the transmitter. Class-D half-bridge or full-bridge topologies have low voltage and current stress on the switches, however, their gate-driver implementation is a big challenge due to the high-side switch referenced to a floating node [9]–[12]. On the other hand, the Class-E inverter has only one switch and it is referenced to the ground, making it easier to design the gate-driver circuit. Moreover, it has higher voltage and current stress than the Class-D counterpart [13]–[16]. In complement, the full potential of the resonant inverters, both Class-D and Class-E and their variants, is achieved by considering their design in optimal operating, i.e., by operating with soft-switching mechanisms as zero-voltage switching (ZVS) or zero-current switching (ZCS).

Considering the design complexity of the Class-E resonant inverter, originating from its soft-switching characteristic, the sinusoidal assumption for the output waveforms is chiefly considered. In [16], a Class-E ZVS inverter with load independence characteristic is analyzed by assuming the loaded quality factor high enough to ensure that the output voltage is represent by a sine function. Also, an inverse Class-E inverter applied to WPT system is design in [17] by using a sinusoid output current. Furthermore, Class-D, Class-E, Class-E^{-1}, Class-DE, Class-EF and constant output Class-E are mostly analyzed in the literature by using the aforementioned assumption [18]–[23].

In this paper, the Class-E resonant inverter is analyzed without assuming the sinusoid output waveform. Thus, the output obtained equations have sine, cosine and exponential terms. The proposed approach enhances the design range and allows to reduce the component values for the magnetic components. It is because the resonant inductor is directly proportional to the quality factor; by setting the output variables as a sinusoid waveform, the quality factor is restrained, limiting the resonant inductor component value. In addition, when considering WPT applications, the inductive coils are considered as an equivalent load for the power inverter. Therefore, by restraining the resonant inductor value, the inductive coils are also confined in an inductance range.

The proposed method consists in the exact solution of the Class-E inverter, which means that, the time-domain solutions are obtained for the, resonant inductor current, parallel capacitor voltage and resonant capacitor voltage, without assuming the output as a sine waveform. By equating the solutions for each operating stage, it is possible to design the hardware components for the WPT application.

In order to model the WPT system, a coupled inductor model based on lumped parameters is presented. In contrast to other approaches, like as the finite element method [24], the proposed WPT representation can be easily connected as an equivalent load to the 1D topology of the converter. Therefore, it is possible to analyze by parameter sweeping the influence of the coils distance into the electrical variables of the power stage.

This paper is organized as follows: In Section II, the Class-E WPT resonant inverter is presented. In Section III, the exact solution is obtained for the targeting electrical variables. The inductive coupling analysis is performed in Section IV. A design methodology is detailed in Section

V. Finally, the experimental results and the conclusions are shown in Section VI and VII, respectively.

II. CLASS-E WPT RESONANT INVERTER

By cascading a Class-E resonant inverter to a wireless power transfer system and modeling the inductive link as an equivalent load, the Class-E WPT resonant inverter in Fig. 1 is obtained. The Class-E inverter is composed of: input voltage V_{in}, choke inductor L_c, switch S, inverter capacitor C_p, resonant inductor L_r and a resonant capacitor C_r. The WPT system models the load for the Class-E inverter, which has a transmitter coil L_1, a receiver coil L_2 and a mutual inductance M. Finally, the system supplies a load R_L. The circuit variables are described as: resonant current i_{L_r}, transmitter loop current $\mathbf{I}_1$, receiver loop current $\mathbf{I}_2$, switch voltage v_S, parallel capacitor voltage v_{C_p}, and resonant capacitor voltage v_{C_r}.

The WPT system can be represented by a coupled inductor model with elements that depend on the angular operating frequency ω. By equating $\mathbf{I}_1$, the input impedance of the inductive link can be found. It is going to be presented that it has a resistance R_{in} part and an inductive reactance represented by an inductor L_{in}. Thus, due to the series connection, the resonant inductor L_r and the WPT system input inductor L_{in} can be replaced by an equivalent inductor $L_{\text{eq}} = L_r + L_{\text{in}}$.

In this sense, the Class-E WPT resonant inverter to be analyzed has the same topology of the standard Class-E inverter as long as due care is taken. Therefore, the following premises are considered in the subsequently analysis: 1) All components are ideal; 2) V_{in} and L_c are replaced by a constant current source, I_{in}; 3) The exact solution is target on the resonant circuit variables, which means i_{L_r}, v_{C_p} and v_{C_r}; 4) The analyzed resonant inductance requires a value that is sufficient to incorporate the transmitter coil inductance value and also has enough inductance for the Class-E inverter implementation. It is because, the converter is analyzed by considering the combination of L_r and L_{in}, therefore, the physical inductor for the Class-E converter is the analyzed inductance in the theoretical approach minus the receiver coil inductance from the WPT system; 5) The converter has two operating stages related to switch S on/off states and defined by duty cycle D_c. In the end of stage II, switch S turns-on with zero-voltage switching (ZVS) and zero-derivative voltage switching (ZDVS); 6) Operating frequency is constant; 7) Steady-state operation. The theoretical waveforms are depicted in Fig. 2 and the equivalent circuits for each operating stage in Fig. 3.

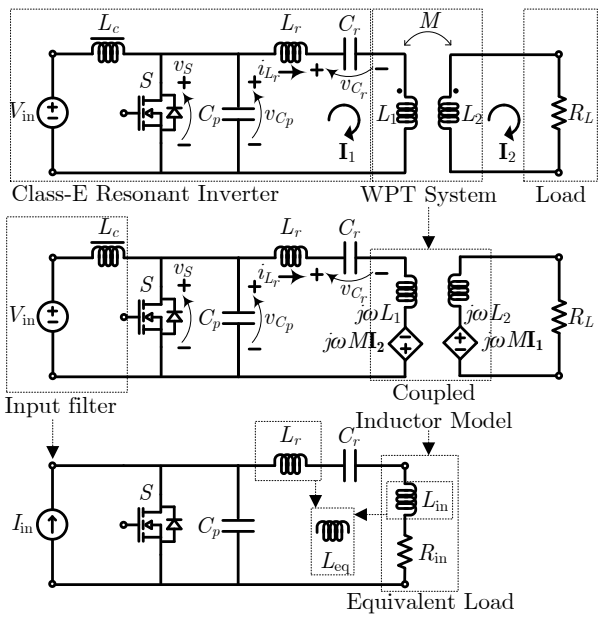

FIGURE 1. Class-E WPT resonant inverter.

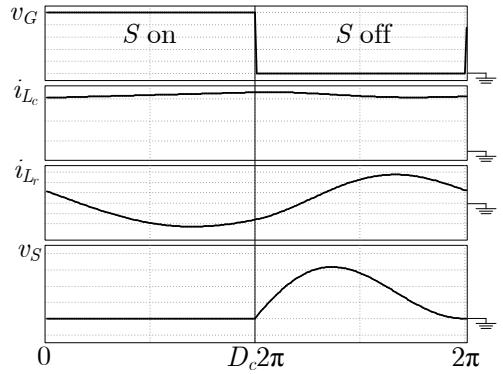

FIGURE 2. Theoretical waveforms.

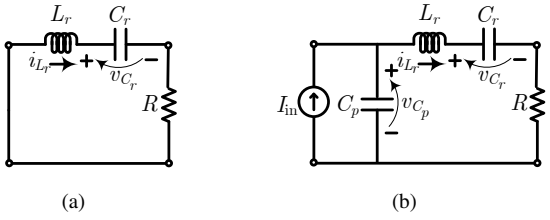

FIGURE 3. Class-E inverter topology. (a) Switch S on. (b) Switch S off.

In the next section, the Class-E resonant inverter is going to be analyzed targeting to find the exact solution for each circuit variable. By finding the time domain solution for the Class-E topology, it is possible to later on design the converter components by considering the equivalent load as a representation of the WPT system as conceptualized in Fig. 1.

III. EXACT SOLUTION OF THE CLASS-E INVERTER

The main concept is to use the reactive element governing equations in the complex frequency domain. The inductor voltage is given by:

$$v_L(t) = L\frac{di_L(t)}{dt} \overset{\mathcal{L}}{\longleftrightarrow} sLI_L(s) - Li_L(0) \qquad (1)$$

and a capacitor voltage:

$$v_C(t) = \frac{1}{C}\int i_C(t)dt \overset{\mathcal{L}}{\longleftrightarrow} \frac{1}{sC}I_C(t) + \frac{1}{s}v_C(0). \quad (2)$$

The loop equation for stage 1 is written as

$$v_{L_r} + v_{C_r} + v_R = 0, \quad (3)$$

which can be expressed by

$$sL_rI_2(s) - L_ri_{L_r}(0) + \frac{I_2(s)}{sC_r} + \frac{v_{C_r}(0)}{s} + I_2(s)R = 0. \quad (4)$$

$I_2(s)$ represents the current in the resonant loop, composed of $C_p - L_r - C_r - R$, and it can be written in terms of the initial conditions, $i_{L_r}(0)$ e $v_{C_r}(0)$, the complex frequency s and the circuit components,

$$I_2(s) = \frac{si_{L_r}(0) - \frac{v_{C_r}(0)}{L_r}}{s^2 + s\frac{R}{L_r} + \frac{1}{L_rC_r}}. \quad (5)$$

Due to the second order polynomial, the completing the square method can be used to rewrite the denominator aiming to find well-known Laplace transformations. Thus, $I_2(s)$ is represented by:

$$I_2(s) = \frac{si_{L_r}(0) - \frac{v_{C_r}(0)}{L_r}}{a_1\left[(s+\alpha_1)^2 + \omega_1^2\right]}, \quad (6)$$

where: $\alpha_1 = \frac{b_1}{2a_1}$, $\omega_1 = \sqrt{\beta_1}$ and $\beta_1 = \frac{c_1}{a_1} - \alpha_1^2$, with the coefficients: $a_1 = 1$, $b_1 = \frac{R}{L_r}$ e $c_1 = \frac{1}{L_rC_r}$.

Equation (6) is algebraically adjusted to find $s+\alpha_1$ in the numerator:

$$\begin{aligned} I_2(s) &= \frac{s - \frac{v_{C_r}(0)}{L_ri_{L_r}(0)}}{\frac{a_1}{i_{L_r}(0)}\left[(s+\alpha_1)^2 + \omega_1^2\right]} \\ &= \frac{s+\alpha_1-\alpha_1}{\frac{a_1}{i_{L_r}(0)}\left[(s+\alpha_1)^2 + \omega_1^2\right]} - \frac{\frac{v_{C_r}(0)}{L_ri_{L_r}(0)}}{\frac{a_1}{i_{L_r}(0)}\left[(s+\alpha_1)^2 + \omega_1^2\right]}. \end{aligned} \quad (7)$$

The first term in (7) is separated into two new terms that are known as cosine and sine portions in the Laplace transformations:

$$\begin{aligned} I_2(s) = &\frac{i_{L_r}(0)}{a_1}\frac{s+\alpha_1}{\left[(s+\alpha_1)^2+\omega_1^2\right]} - \frac{i_{L_r}(0)\alpha_1}{a_1\omega_1}\frac{\omega_1}{\left[(s+\alpha_1)^2+\omega_1^2\right]} \\ &- \frac{v_{C_r}(0)}{a_1L_r\omega_1}\frac{\omega_1}{\left[(s+\alpha_1)^2+\omega_1^2\right]}. \end{aligned} \quad (8)$$

By applying the Inverse Laplace Transform by means of the direct replacement of the well-known transformations, the time domain solution can be achieved:

$$\begin{aligned} \overset{\text{I}}{i}_{L_r}(t) = &\frac{i_{L_r}(0)}{a_1}\mathrm{e}^{-\alpha_1 t}\cos(\omega_1 t) - \frac{i_{L_r}(0)\alpha_1}{a_1\omega}\mathrm{e}^{-\alpha_1 t}\sin(\omega_1 t) \\ &- \frac{v_{C_r}(0)}{a_1L_r\omega}\mathrm{e}^{-\alpha_1 t}\sin(\omega_1 t)\,\mathrm{A}. \end{aligned} \quad (9)$$

Equation (9) describes the exact solution of the loop current I_2 in time domain, which also describes the current $i_{L_r}(t)$ in the resonant inductor L_r. The upper-script I denotes the first operating stage.

Since the switch S is turned-on in the first stage, the parallel capacitor voltage is zero. Therefore:

$$\overset{\text{I}}{v}_{C_p}(t) = 0\,\mathrm{V}. \quad (10)$$

The resonant capacitor voltage v_{C_r} in the complex frequency domain can be obtained by considering $I_2(s)$, described by (5), times $1/(sC_r)$:

$$V_{C_r}(s) = \frac{1}{sC_r}I_2(s) + \frac{1}{s}v_{C_r}(0), \quad (11)$$

ergo,

$$V_{C_r}(s) = \left(\frac{1}{sC_r}\right)\left(\frac{si_{L_r}(0) - \frac{v_{C_r}(0)}{L_r}}{s^2 + s\frac{R}{L_r} + \frac{1}{L_rC_r}}\right) + \frac{v_{C_r}(0)}{s}. \quad (12)$$

Due to the polynomial multiplication in the first term of (12), it is necessary to apply partial fractions by considering the finding constants A_1, A_2 and B_2,

$$V_{C_r}(s) = \frac{1}{C_r}\left(\frac{A_1}{s+0} + \frac{A_2s + B_2}{s^2 + s\frac{R}{L_r} + \frac{1}{L_rC_r}}\right) + \frac{v_{C_r}(0)}{s}, \quad (13)$$

hence,

$$\begin{aligned} V_{C_r}(s) = &\frac{1}{C_r}\left[\frac{A_1s^2 + A_1s\frac{R}{L_r} + A_1\frac{1}{L_rC_r} + A_2s^2 + B_2s}{(s+0)\left(s^2 + s\frac{R}{L_r} + \frac{1}{L_rC_r}\right)}\right] \\ &+ \frac{v_{C_r}(0)}{s}. \end{aligned} \quad (14)$$

Therefore, the following linear system is considered:

$$\begin{cases} A_1 + A_2 = 0 \\ A_1\frac{R}{L_r} + B_2 = i_{L_r}(0) \\ A_1\frac{1}{L_rC_r} = -\frac{v_{C_r}(0)}{L_r} \end{cases}, \quad (15)$$

which returns $A_1 = -C_rv_{C_r}(0)$, $A_2 = C_rv_{C_r}(0)$ and $B_2 = \frac{L_ri_{L_r}(0) + RC_rv_{C_r}(0)}{L_r}$. A_1, A_2 and B_2 are replaced in (14):

$$\begin{aligned} V_{C_r}(s) = &-v_{C_r}(0)\left(\frac{1}{s+0}\right) + v_{C_r}(0)\left(\frac{s}{s^2 + s\frac{R}{L_r} + \frac{1}{L_rC_r}}\right) \\ &+ \frac{L_ri_{L_r}(0) + RC_rv_{C_r}(0)}{L_rC_r}\left(\frac{s}{s^2 + s\frac{R}{L_r} + \frac{1}{L_rC_r}}\right) \\ &+ \frac{v_{C_r}(0)}{s}. \end{aligned} \quad (16)$$

The same completing the square that was applied in the resonant current i_{L_r} analysis is used in the resonant capacitor voltage v_{C_r}. In addition, the terms should be arranged aiming to find the Laplace transformations. Therefore:

$$\begin{aligned} V_{C_r}(s) = &-v_{C_r}(0)\left(\frac{1}{s}\right) + \frac{v_{C_r}(0)}{a_1}\left(\frac{s+\alpha_1}{\left[(s+\alpha_1)^2+\omega_1^2\right]}\right) \\ &- \frac{v_{C_r}(0)\alpha_1}{a_1\omega_1}\left(\frac{\omega_1}{\left[(s+\alpha_1)^2+\omega_1^2\right]}\right) \\ &+ \frac{L_ri_{L_r}(0) + RC_rv_{C_r}(0)}{L_rC_ra_1\omega_1}\left(\frac{\omega_1}{\left[(s+\alpha_1)^2+\omega_1^2\right]}\right) \\ &+ \frac{v_{C_r}(0)}{s}. \end{aligned} \quad (17)$$

Finally, the equation can be converted to the time domain as:

$$\begin{aligned} v_{C_r}^{\text{I}}(t) =& \frac{v_{C_r}(0)}{a_1}\mathrm{e}^{-\alpha_1 t}\cos(\omega_1 t) - \frac{v_{C_r}(0)\alpha_1}{a_1\omega_1}\mathrm{e}^{-\alpha_1 t}\sin(\omega_1 t) \\ &+ \frac{L_r i_{L_r}(0) + RC_r v_{C_r}(0)}{L_r C_r a_1 \omega_1}\mathrm{e}^{-\alpha_1 t}\sin(\omega_1 t)\,\text{V}. \end{aligned} \tag{18}$$

In the stage II, switch S is off and the circuit shown in Fig. 3(b) should be considered. In order to find the resonant current, the loop equation is used as follows

$$-v_{C_p} + v_{L_r} + v_{C_r} + v_R = 0, \tag{19}$$

so

$$\begin{aligned} &-\frac{1}{sC_p}\left[I_1(s) - I_2(s)\right] - \frac{1}{s}v_{C_p}(D_cT) + sL_rI_2(s) \\ &-L_r i_{L_r}(D_cT) + \frac{1}{sC_r}I_2(s) + \frac{1}{s}v_{C_r}(D_cT) + I_2(s)R = 0. \end{aligned} \tag{20}$$

One can see that the initial conditions for stage II are related to the instant D_cT, where T is the period. In addition, $I_1(s) = \frac{I_{\text{in}}}{s}$. Equating $I_2(s)$:

$$I_2(s) = \frac{\frac{I_{\text{in}}}{s}\frac{1}{sC_p} + L_r i_{L_r}(D_cT) - \frac{v_{C_r}(D_cT)}{s}}{sL_r + \frac{1}{sC_r} + R + \frac{1}{sC_p}}, \tag{21}$$

which should be adjusted as

$$I_2(s) = \left[\frac{1}{s}\right]\left[\frac{s^2L_rC_pC_r i_{L_r}(D_cT) - sC_pC_r v_{C_r}(D_cT) + I_{\text{in}}C_r}{s^2L_rC_pC_r + sRC_pC_r + (C_r + C_p)}\right]. \tag{22}$$

By applying partial fraction decomposition considering one linear term and one quadratic term, the following is obtained:

$$I_2(s) = \frac{A_1}{s+0} + \frac{A_2 s + B_2}{s^2L_rC_pC_r + sRC_pC_r + (C_r + C_p)}, \tag{23}$$

then,

$$I_2(s) = \frac{s^2L_rC_pC_rA_1 + sRC_pC_rA_1 + (C_r + C_p)A_1 + s^2A_2 + sB_2}{(s+0)(s^2L_rC_pC_r + sRC_pC_r + C_r + C_p)}. \tag{24}$$

The following system of equations should be solved in order to find the constants:

$$\begin{cases} L_rC_pC_rA_1 + A_2 = L_rC_pC_r i_{L_r}(D_cT) \\ RC_pC_rA_1 + B_2 = -C_pC_r v_{C_r}(D_cT) \\ (C_r + C_p)A_1 = I_{\text{in}}C_r \end{cases}, \tag{25}$$

which leads to

$$A_1 = \frac{I_{\text{in}}C_r}{C_p + C_r}, \tag{26}$$

$$A_2 = \frac{-I_{\text{in}}C_pC_r^2L_r + C_p^2C_rL_r i_{L_r}(D_cT) + C_pC_r^2L_r i_{L_r}(D_cT)}{C_p + C_r} \tag{27}$$

and

$$B_2 = \frac{-I_{\text{in}}C_pC_r^2R - C_p^2C_r v_{C_r}(D_cT) - C_pC_r^2 v_{C_r}(D_cT)}{C_p + C_r}. \tag{28}$$

By replacing A_1, A_2 e B_2:

$$\begin{aligned} I_2(s) =& \frac{I_{\text{in}}C_r}{C_p + C_r}\left(\frac{1}{s+0}\right) \\ &+ \frac{-I_{\text{in}}C_pC_r^2L_r + C_p^2C_rL_r i_{L_r}(D_cT) + C_pC_r^2L_r i_{L_r}(D_cT)}{C_p + C_r} \\ &\times\left(\frac{s}{s^2L_rC_pC_r + sRC_pC_r + (C_r + C_p)}\right) \\ &+ \frac{-I_{\text{in}}C_pC_r^2R - C_p^2C_r v_{C_r}(D_cT) - C_pC_r^2 v_{C_r}(D_cT)}{C_p + C_r} \\ &\times\left(\frac{1}{s^2L_rC_pC_r + sRC_pC_r + (C_r + C_p)}\right), \end{aligned} \tag{29}$$

which is rewritten by the completing the square method as

$$\begin{aligned} I_2(s) =& \frac{I_{\text{in}}C_r}{C_p + C_r}\left(\frac{1}{s+0}\right) \\ &+ \frac{-I_{\text{in}}C_pC_r^2L_r + C_p^2C_rL_r i_{L_r}(D_cT) + C_pC_r^2L_r i_{L_r}(D_cT)}{C_p + C_r} \\ &\times\left(\frac{s}{a_2\left[(s+\alpha_2)^2 - \omega_2^2\right]}\right) \\ &+ \frac{-I_{\text{in}}C_pC_r^2R - C_p^2C_r v_{C_r}(D_cT) - C_pC_r^2 v_{C_r}(D_cT)}{C_p + C_r} \\ &\times\left(\frac{1}{a_2\left[(s+\alpha_2)^2 - \omega_2^2\right]}\right), \end{aligned} \tag{30}$$

where $\alpha_2 = \frac{b_2}{2a_2}$, $\omega_2 = \sqrt{-\beta_2}$ and $\beta_2 = \frac{c_2}{a_2} - \alpha_2^2$ with coefficients: $a_2 = L_rC_pC_r$, $b_2 = RC_pC_r$ e $c_2 = C_r + C_p$.

By adjusting the terms in order to find the Laplace transformations, $I_2(s)$ becomes

$$\begin{aligned} I_2(s) =& \frac{I_{\text{in}}C_r}{C_p + C_r}\left(\frac{1}{s}\right) \\ &+ \frac{-I_{\text{in}}C_pC_r^2L_r + C_p^2C_rL_r i_{L_r}(D_cT) + C_pC_r^2L_r i_{L_r}(D_cT)}{C_p + C_r} \\ &\times\frac{1}{a_2}\left(\frac{s+\alpha_2}{\left[(s+\alpha_2)^2 - \omega_2^2\right]}\right) \\ &- \frac{-I_{\text{in}}C_pC_r^2L_r + C_p^2C_rL_r i_{L_r}(D_cT) + C_pC_r^2L_r i_{L_r}(D_cT)}{C_p + C_r} \\ &\times\frac{\alpha_2}{a_2\omega_2}\left(\frac{\omega_2}{\left[(s+\alpha_2)^2 - \omega_2^2\right]}\right) \\ &+ \frac{-I_{\text{in}}C_pC_r^2R - C_p^2C_r v_{C_r}(D_cT) - C_pC_r^2 v_{C_r}(D_cT)}{C_p + C_r} \\ &\times\frac{1}{a_2\omega_2}\left(\frac{\omega_2}{a_2\left[(s+\alpha_2)^2 - \omega_2^2\right]}\right). \end{aligned} \tag{31}$$

In this configuration, the Inverse Laplace Transform can be applied. The time-domain exact equation for the resonant current in stage II is obtained as:

$$\begin{aligned}
\overset{\text{II}}{i}_{L_r}(t) =& \frac{I_{\text{in}}C_r}{C_p+C_r} \\
&+\frac{-I_{\text{in}}C_pC_r^2L_r+C_p^2C_rL_ri_{L_r}(D_cT)+C_pC_r^2L_ri_{L_r}(D_cT)}{C_p+C_r} \\
&\times\frac{1}{2a_2}\left(\mathrm{e}^{-(\alpha_2-\omega_2)t}+\mathrm{e}^{-(\alpha_2+\omega_2)t}\right) \\
&-\frac{-I_{\text{in}}C_pC_r^2L_r+C_p^2C_rL_ri_{L_r}(D_cT)+C_pC_r^2L_ri_{L_r}(D_cT)}{C_p+C_r} \\
&\times\frac{\alpha_2}{2a_2\omega_2}\left(\mathrm{e}^{-(\alpha_2-\omega_2)t}-\mathrm{e}^{-(\alpha_2+\omega_2)t}\right) \\
&+\frac{-I_{\text{in}}C_pC_r^2R-C_p^2C_rv_{C_r}(D_cT)-C_pC_r^2v_{C_r}(D_cT)}{C_p+C_r} \\
&\times\frac{1}{2a_2\omega_2}\left(\mathrm{e}^{-(\alpha_2-\omega_2)t}-\mathrm{e}^{-(\alpha_2+\omega_2)t}\right)\text{A}.
\end{aligned} \tag{32}$$

In stage II, switch S is off, so, there is voltage in capacitor C_p. The frequency domain equation for its voltage is

$$v_{C_p}(s)=\frac{I_1(s)-I_2(s)}{sC_p}+\frac{v_{C_p}(D_cT)}{s}, \tag{33}$$

then

$$\begin{aligned}
v_{C_p}(s) =& \frac{I_{\text{in}}}{s^2C_p}-\left(\frac{1}{sC_p}\right)\left(\frac{1}{s}\right) \\
&\times\left(\frac{s^2L_rC_pC_ri_{L_r}(D_cT)-sC_pC_rv_{C_r}(D_cT)+I_{\text{in}}C_r}{s^2L_rC_pC_r+sRC_pC_r+C_r+C_p}\right).
\end{aligned} \tag{34}$$

The same procedure shown for the resonant inductor analysis should be applied in (34), which consists of: partial fraction decomposition, completing the square method and Inverse Laplace Transform. The terms α_2, ω_2 e a_2 are the same terms obtained in the inductor L_r equating for stage II.

The analysis for capacitor C_r is the same as shown for capacitor C_p, except for the influence of current $I_1(s)$. Note that, the loop current $I_1(s)$ is the same as the DC input current I_{in}. Therefore, the parallel capacitor voltage in stage II and the time-domain exact equation for $v_{C_r}(t)$ in stage II are shown in (35) and (36), respectively.

The provided exact solution of the Class-E WPT converter is related to its resonant electrical variables: resonant current $i_{L_r}(t)$, parallel capacitor voltage $v_{C_p}(t)$ and resonant capacitor voltage $v_{C_r}(t)$. The proposed methodology has the following features:

1) The exact solution of $i_{L_r}(t)$ is not limited to the high load quality factor, i.e., the solution is not limited to the sinusoidal approximation;
2) The resonant inductor L_r and load R can be evaluated considering the equivalent input impedance of the WPT system. Therefore, allowing to investigate the converter behavior considering the inductive coupling;
3) By performing a parameter sweeping and considering the steady-state conditions, the power stage can be designed based on the exact time-domain equations.

$$\begin{aligned}
\overset{\text{II}}{v}_{C_p}(t) =& \frac{I_{\text{in}}}{C_p}t+\frac{I_{\text{in}}C_r^2R+C_pC_rv_{C_r}(D_cT)+C_r^2v_{C_r}(D_cT)}{(C_p+C_r)^2} \\
&-\frac{1}{C_p}\frac{I_{\text{in}}C_r}{C_p+C_r}t \\
&-\frac{C_pL_r\left[I_{\text{in}}C_r^3R+C_pC_r^2v_{C_r}(D_cT)+C_r^3v_{C_r}(D_cT)\right]}{(C_p+C_r)^2} \\
&\times\frac{1}{2a_2}\left(\mathrm{e}^{-(\alpha_2-\omega_2)t}+\mathrm{e}^{-(\alpha_2+\omega_2)t}\right) \\
&+\frac{C_pL_r\left[I_{\text{in}}C_r^3R+C_pC_r^2v_{C_r}(D_cT)+C_r^3v_{C_r}(D_cT)\right]}{(C_p+C_r)^2} \\
&\times\frac{\alpha_2}{2a_2\omega_2}\left(\mathrm{e}^{-(\alpha_2-\omega_2)t}-\mathrm{e}^{-(\alpha_2+\omega_2)t}\right)+\frac{1}{C_p} \\
&\times\left[\frac{I_{\text{in}}C_p^2C_r^2L_r+I_{\text{in}}C_pC_r^3L_r-C_p^3C_rL_ri_{L_r}(D_cT)}{(C_p+C_r)^2}\right. \\
&-\frac{2C_p^2C_r^2L_ri_{L_r}(D_cT)+C_pC_r^3L_ri_{L_r}(D_cT)+I_{\text{in}}C_p^2C_r^3R^2}{(C_p+C_r)^2} \\
&\left.+\frac{-C_p^3C_r^2Rv_{C_r}(D_cT)-C_p^2C_r^3Rv_{C_r}(D_cT)}{(C_p+C_r)^2}\right] \\
&\times\frac{1}{a_2\omega_2}\left(\mathrm{e}^{-(\alpha_2-\omega_2)t}-\mathrm{e}^{-(\alpha_2+\omega_2)t}\right)\text{V}.
\end{aligned} \tag{35}$$

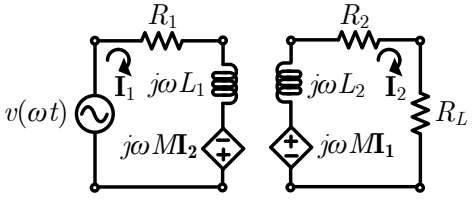

FIGURE 4. Coupled inductor model.

$$
\begin{aligned}
v_{C_r}^{\text{II}}(t) = &- \frac{C_p}{C_r}\frac{I_{\text{in}}C_r^2R + C_pC_rv_{C_r}(D_cT) + C_r^2v_{C_r}(D_cT)}{(C_p+C_r)^2} \\
&+ \frac{I_{\text{in}}C_r}{C_p+C_r}t \\
&+ \frac{C_p^2L_r\left[I_{\text{in}}C_r^3R + C_pC_r^2v_{C_r}(D_cT) + C_r^3v_{C_r}(D_cT)\right]}{(C_p+C_r)^2} \\
&\times \frac{1}{2a_2}\left(\mathrm{e}^{-(\alpha_2-\omega_2)t} + \mathrm{e}^{-(\alpha_2+\omega_2)t}\right) \\
&- \frac{C_p^2L_r\left[I_{\text{in}}C_r^3R + C_pC_r^2v_{C_r}(D_cT) + C_r^3v_{C_r}(D_cT)\right]}{(C_p+C_r)^2} \\
&\times \frac{\alpha_2}{2a_2\omega_2}\left(\mathrm{e}^{-(\alpha_2-\omega_2)t} - \mathrm{e}^{-(\alpha_2+\omega_2)t}\right) \\
&- \left[\frac{I_{\text{in}}C_p^2C_r^2L_r + I_{\text{in}}C_pC_r^3L_r - C_p^3C_rL_ri_{L_r}(D_cT)}{(C_p+C_r)^2}\right. \\
&- \frac{2C_p^2C_r^2L_ri_{L_r}(D_cT) + C_pC_r^3L_ri_{L_r}(D_cT) + I_{\text{in}}C_p^2C_r^3R^2}{(C_p+C_r)^2} \\
&\left. + \frac{-C_p^3C_r^2Rv_{C_r}(D_cT) - C_p^2C_r^3Rv_{C_r}(D_cT)}{(C_p+C_r)^2}\right] \\
&\times \frac{1}{a_2\omega_2}\left(\mathrm{e}^{-(\alpha_2-\omega_2)t} - \mathrm{e}^{-(\alpha_2+\omega_2)t}\right)\text{V}.
\end{aligned}
\tag{36}
$$

IV. INDUCTIVE COUPLING ANALYSIS

In order to find an equivalent circuit for the inductive coupling aiming to use it as load for the Class-E inverter, Fig. 4 shows the coupled inductor model to be analyzed. R_1 and R_2 represent the coil losses. In addition, the input voltage source $v(\omega t)$ is represented in the rectangular phasor form with real part x_1 and imaginary part y_1, i.e., $v(\omega t) = x_1 + jy_1$.

The following equation are obtained by applying KVL in the first loop:

$$-(x_1 + jy_1) + \mathbf{I}_1(R_1 + j\omega L_1) - \mathbf{I}_2(j\omega M) = 0, \tag{37}$$

which leads to

$$\mathbf{I}_1(R_1 + j\omega L_1) - \mathbf{I}_2(j\omega M) = (x_1 + jy_1). \tag{38}$$

The same procedure is used in the second loop,

$$-j\omega M\mathbf{I}_1 + \mathbf{I}_2(R_2 + j\omega L_2) + \mathbf{I}_2R_L = 0. \tag{39}$$

then,

$$\mathbf{I}_1(-j\omega M) + \mathbf{I}_2(R_2 + R_L + j\omega L_2) = 0. \tag{40}$$

Equations (38) and (40) provides a linear system of equations, which returns the symbolical expressions for $\mathbf{I}_1$ and $\mathbf{I}_2$. Loop current $\mathbf{I}_1$ is found as

$$\mathbf{I}_1 = \frac{(-x_1 - jy_1)(R_2 + R_L + j\omega L_2)}{-M^2\omega^2 - (R_1 + j\omega L_1)(R_2 + R_L + j\omega L_2)}. \tag{41}$$

The input impedance of the inductive coupling can be calculated by

$$Z_{in} = \frac{x_1 + y_1 j}{\mathbf{I}_1}, \tag{42}$$

which can be used as an equivalent load for the inverter stage.

Finally, the relation between the mutual inductance M, considering two coils with diameters D_1 and D_2, and the transmitter-receiver distance d, can be mathematically expressed by [25]

$$M = \mu_o N_1 N_2 \sqrt{\frac{D_1D_2}{4}}\left[\left(\frac{2}{k} - k\right)K_1(k) - \frac{2}{k}E_1(k)\right], \tag{43}$$

being μ_0 (H/m) the material permeability, $N_{1,2}$ the winding number and $K_1(k)$ e $E_1(k)$ are the complete elliptic integrals of the first kind and second kind, respectively. In addition, k is described as

$$k = \sqrt{\frac{D_1D_2}{d^2 + \left(\frac{D_1}{2} + \frac{D_1}{2}\right)^2}}. \tag{44}$$

V. DESIGN METHODOLOGY

The design of the Class-E WPT converter is performed in two parts: 1) The input impedance of the WPT system should be calculated based on the geometry and physical properties of the transmitter and receiver coils and electrical design specifications; 2) The Class-E resonant inverter component values are calculated based on a linear system of equations developed from the exact time-domain equations. The transmitter and receiver coil parameters are described in Table 1. In addition, $\mu_o = 4\pi 10^{-7}$ H/m.

TABLE 1. Inductive Coil Parameters.

Parameter	Value
Primary side winding number, N_1	10
Secondary side winding number, N_2	5
Coil diameter $D_{1,2}$	50 mm
Primary side losses, R_1	180 mΩ
Secondary side losses, R_2	145 mΩ
Primary side inductance, L_1	7.7 μH
Secondary side inductance, L_2	3.4 μH

The mutual inductance can be calculated by Equation (43). However, it requires a numerical solution. Table 2 and 3 show M as function of coil distance d for distances less than 10 mm and greater than 10 mm, respectively.

TABLE 2. Numerical Solution: M as function of d ($d < 10$ mm).

M (μH)	4.65	4.06	3.44	3.01	2.67	2.40	2.18	1.99	1.82
d (mm)	1	2	3	4	5	6	7	8	9

TABLE 3. Numerical Solution: M as function of d ($d > 10$ mm).

M (μH)	1.68	0.83	0.46	0.27	0.17	0.11	0.08	0.05	0.04
d (mm)	10	20	30	40	50	60	70	80	90

In order to design the system, the highest power transfer situation is considered, which means $M = 4.65\,\mu$H. In addition, the electrical design specifications are considered

as: operating frequency $f_s = 500\,\text{kHz}$ output power $P_L = 5\,\text{W}$, inverter output RMS voltage $V_{L_{\text{RMS}}} = 14\,\text{V}$. Hence, $\mathbf{I}_1$ can be calculated by Equation (41), which results on $\mathbf{I}_1 = 0.622 - 2.705j\,\text{A}$, then, by defining the transmitter coil input voltage in rectangular coordinate, for instance $x_1 = 65$ and $y_1 = 0.0068j$, the input impedance is found as $Z_{\text{in}} = 5.25 + 23j\,\Omega$.

By calculating the input impedance of inductive coils, it can be represented by an equivalent load for the Class-E inverter. The real part represents a resistance $R_{\text{in}} = 5.25\,\Omega$. On the other hand, the positive imaginary part denotes an inductive reactance $\mathbf{X}_{\text{in}}$. The equivalent inductor is calculated as

$$L_{\text{in}} = \frac{\mathbf{X}_{\text{in}} j}{\omega j} = 7.271\,\mu H. \tag{45}$$

Considering the equivalent load R_{in}-L_{in} for the Class-E inverter, it is possible to design the power stage components by means of the exact time-domain equations. By equating the solutions for stage II replacing time t for T, i.e., the end of one cycle, to the symbolical initial conditions, a linear system of equations can be built, which represents the steady-state operation. In addition, the soft-switching conditions can be incorporated. Therefore:

$$\begin{pmatrix} \overset{\text{II}}{i_{L_r}}(T) \\ \overset{\text{II}}{v_{C_r}}(T) \\ \overset{\text{II}}{v_{C_p}}(T) \\ \overset{\text{II}}{i_{L_r}}(T) \\ \overset{\text{I}}{i_{L_r}}(D_cT) \\ \overset{\text{I}}{v_{C_r}}(D_cT) \end{pmatrix} - \begin{pmatrix} i_{L_r}(0) \\ v_{C_r}(0) \\ 0 \\ I_{\text{in}} \\ i_{L_r}(D_cT) \\ v_{C_r}(D_cT) \end{pmatrix} = \begin{pmatrix} 0 \\ 0 \\ 0 \\ 0 \\ 0 \\ 0 \end{pmatrix}. \tag{46}$$

The system in (46) considers the the steady-state operation represented by the two first lines. In the end of a cycle, switch S turns-on with ZVS and ZDVS, indicated by the third and fourth lines, respectively. In addition, the exact solutions for stage I are equated to the initial conditions of stage II. Therefore, there are 6 equations but 13 unknowns: the reactive components, L_r, C_r and C_p; the initial conditions for stage I, $i_{L_r}(0)$, $v_{C_r}(0)$ and $v_{C_p}(0)$; the initial conditions for stage II, $i_{L_r}(D_cT)$, $v_{C_r}(D_cT)$ and $v_{C_p}(D_cT)$; duty cycle D_c, period T, input current I_{in} and load R. Due to the soft-switching operating, $v_{C_p}(0) = v_{C_p}(D_cT) = 0$, which reduces two unknowns. In addition, $T = 1/f_s$, I_{in} and $R = R_{\text{in}}$ are defined because they can be used as design specification. L_r is also defined based on L_{in}. Therefore, by sweeping duty cycle D_c, the values for capacitors C_p and C_r and the initial conditions $i_{L_r}(0)$, $v_{C_r}(0)$, $i_{L_r}(D_cT)$, $v_{C_r}(D_cT)$ are found. The system of linear equations in (46) was solved in a computational implementation by considering the design specifications in Table 4. The system was solved by different values of D_c and the results are shown in Table 5.

TABLE 4. Design Specifications.

Parameter	Value
Operating frequency, f_s	500 kHz
Equivalent inductance, L_{eq}	8.4 μH
Resistive load, R	5.25 Ω
Duty cycle, D_c	$0.3 - 0.7$
Input DC current, I_{in}	1.19 A

TABLE 5. Design Results.

Duty cycle	C_p	C_r	$i_{L_r}(0)$	$v_{C_r}(0)$	$i_{L_r}(D_cT)$	$v_{C_r}(D_cT)$
0.3	12.7 nF	42.8 nF	1.0 A	102.06 V	−4.78 A	70.42 V
0.4	14.8 nF	21.8 nF	1.0 A	61.23 V	−2.70 A	8.92 V
0.5	12.7 nF	16.2 nF	1.0 A	43.76 V	−1.33 A	−19.8 V
0.6	8.41 nF	14.5 nF	1.0 A	30.96 V	−0.41 A	−25.8 V
0.7	4.12 nF	13.4 nF	1.0 A	22.77 V	0.20 A	−23.3 V

The exact solution can be used in the semiconductor sizing. By evaluating the maximum value of the parallel capacitor voltage from $\overset{\text{I}}{v_{C_p}}(t)$ and $\overset{\text{I}}{v_{C_p}}(t)$, and the average value from $I_{\text{in}} - \overset{\text{I}}{i_{L_r}}(t)$, the maximum switch voltage and the average switch current can be obtained for any operating point.

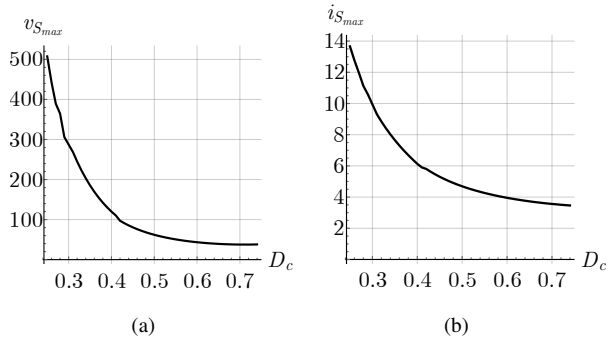

(a) (b)

FIGURE 5. Switch S maximum values as function of D_c. (a) Voltage. (b) Current.

The higher the duty cycle, higher the switch stress. On the other hand, a lower duty cycle provides higher output voltage and less distortion in the resonant current. Therefore, a trade-off must be considered while designing the converter. In this sense, the operating point was selected as $D_c = 0.5$. A circuit simulation was performing considering the design result for $D_c = 0.5$ from Table 5. Furthermore, the choke inductor was calculated as $L_c = \frac{2R}{f_s}$.

The switch stress and output voltage can be also evaluated regarding the distance between the coils. In this sense, by relating the coupled inductor analysis to the exact solution, the charts in Fig. 6 are obtained. Farther the distance d, smaller is the transferred RMS voltage and maximum switch voltage, as depicted in Fig. 6(a) and in Fig. 6(b).

The simulation results are shown in Fig. 7 for gate signal v_{G}, switch voltage v_S, parallel capacitor current i_{C_p}, resonant

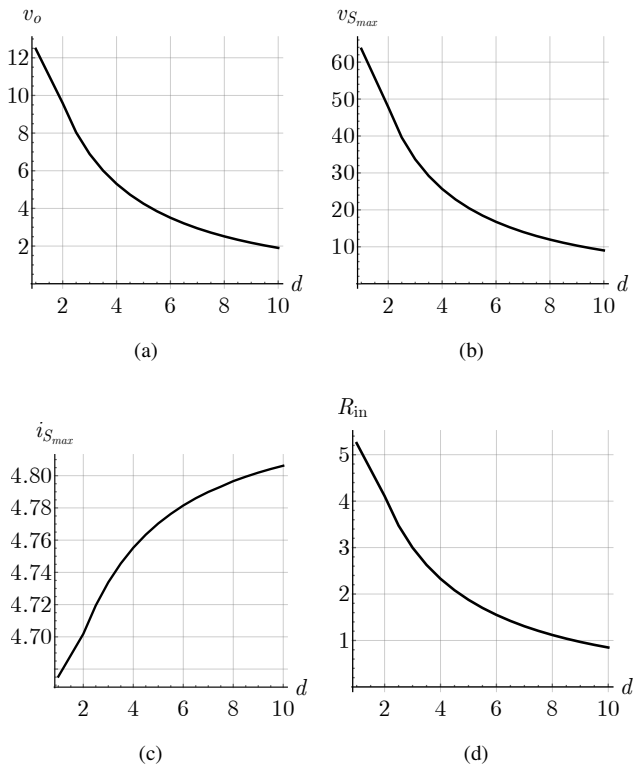

FIGURE 6. Evaluating over distance $d(\mathbf{mm})$. (a) Output RMS voltage $(\mathbf{V})$. (b) Maximum switch voltage $(\mathbf{V})$. (c) Maximum switch current $(\mathbf{A})$. (d) Equivalent WPT input resistance (Ω).

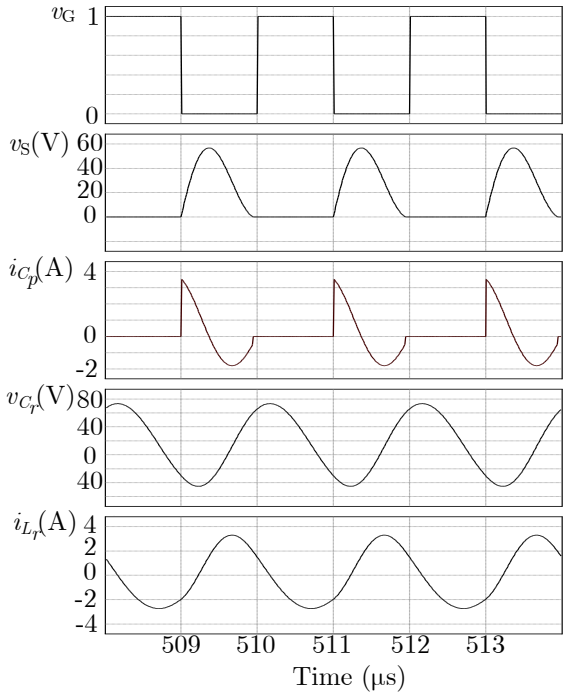

FIGURE 7. Simulation results.

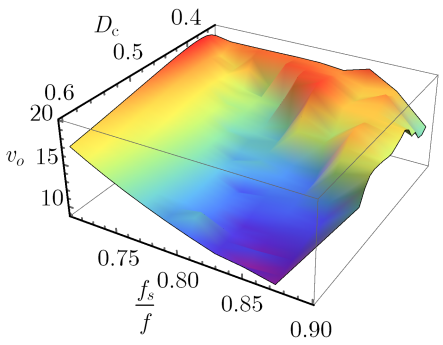

FIGURE 8. 3D mapping of the relation among v_o, D_c and f_s/s.

capacitor voltage v_{C_r} and resonant current i_{L_r}. Besides demonstrating the correct behavior of the converter, the simulation results are used to select commercial capacitors. For C_p, it is taken on consideration the switch voltage maximum value and the capacitor RMS current, which are, $56.6\,\text{V}$ and $1.18\,\text{A}$, respectively. As for C_r, it is considered the capacitor maximum voltage and the resonant RMS current, $73.3\,\text{V}$ and $2.13\,\text{A}$.

The 3D mapping that relates the output voltage (RMS), normalized frequency and duty cycle is depicted in Fig. 8. One can observe the transferred output voltage over different operating points. The normalized frequency was obtained by sweeping the equivalent input inductance of the WPT system and then using its values to calculate f_s/f based on a fixed value for C_r.

VI. EXPERIMENTAL RESULTS

Aiming to experimentally validate the system, the Class-E resonant inverter was implemented in a printed circuit board and a WPT system was built based on transmitter and receiver coils. The hardware components are described in Table 6. Fig. 9 shows the experimental setup, which includes the Class-E inverter and WPT system. The system was tested considering different scenarios regarding distance and output load. The measured output voltage, i.e., the received voltage in the secondary side, is shown in Fig. 10 by considering distances between transmitter and receiver of $1\,\text{mm}$, $2.5\,\text{mm}$, $5\,\text{mm}$ and $10\,\text{mm}$. It can be see that, the greater the distance, lower is the output voltage. Considering $d = 1\,\text{mm}$, the RMS output voltage is $9.83\,\text{V}$. Furthermore, aiming to validate the ZVS operation, Fig. 11 presents the measured gate signal and switch S voltage for different distances. One can see that the switch S voltage reaches zero before the gate signal changes from low to high. The ZVS is maintained from tested distances between $1\,\text{mm}$ and $10\,\text{mm}$.

The Class-E WPT converter was tested also by varying the output power. In this regard, Fig. 12 depicts the efficiency as function of the output power. This evaluation was performed by considering the minimum distance between coils, which means, $d = 1\,\text{mm}$. The highest achieved efficiency was $74\,\%$.

TABLE 6. Hardware Components.

Component/Parameter	Value	Part number/Manufacturer
Choke inductor, L_c	180 μH	Handcrafted
Parallel capacitor, C_p	12 nF	KEMET
Resonant inductor, L_r	1.2 μH	Handcrafted
Resonant capacitor, C_r	15 nF	KEMET
Switch, S	-	IPP530N15N3G
Switch gate-driver	-	IRS2011PBF
PCB size	8 mm × 6 mm	-
Transmitter coil, L_1	7.7 μH	Handcrafted
Receiver coil, L_2	3.4 μH	Handcrafted
Coil diameter, $D_{1,2}$	50 mm	-
Nominal input voltage, V_{in}	15.5 V	-
Operating frequency, f_s	500 kHz	-
Duty cycle, D_c	0.5	-
Load, R_{L}	$4.7 - 24\,\Omega$	-

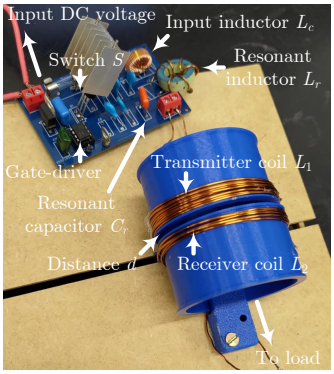

FIGURE 9. Experimental setup.

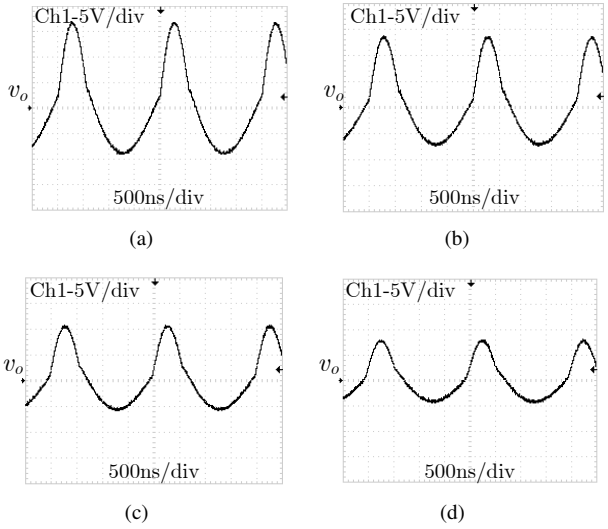

FIGURE 10. Output voltage v_o. (a) $d < 1$ mm. (b) $d = 2.5$ mm. (c) $d = 5$ mm. (d) $d = 10$ mm.

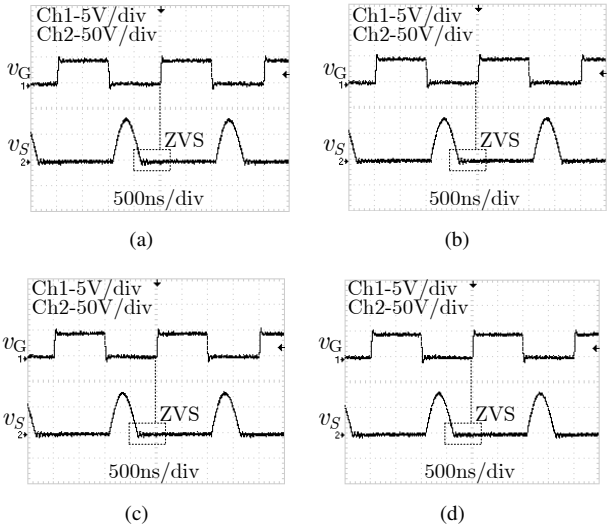

FIGURE 11. Gate signal v_G and switch voltage v_S. (a) $d < 1$ mm. (b) $d = 2.5$ mm. (c) $d = 5$ mm. (d) $d = 7.5$ mm.

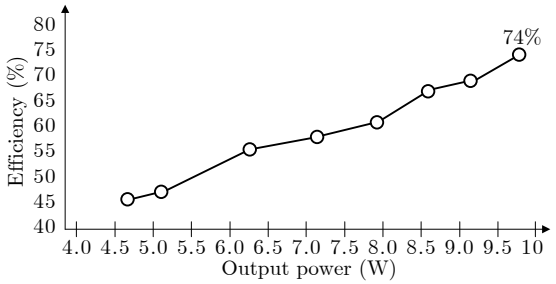

FIGURE 12. Efficiency as function of the output power P_o.

VII. CONCLUSION

In this work, the exact solution of the Class-E WPT resonant inverter has been introduced. The inductive coupling of the WPT system was represented as a RL equivalent load for the Class-E inverter, which allows to analyze the converter in its standard configuration. The exact time-domain solution was obtained for the resonant inductor current, resonant capacitor voltage and parallel capacitor voltage. By using the proposed approach, it is possible to design the hardware components without restraining the quality factor. An experimental setup was built to verify the theory. A 500 kHz ZVS Class-E inverter was designed to drive a WPT system with 50 mm coil diameter. The conclusions are drawn based on the comparison to related works shown in Table 7.

Class-E topologies have only one switch, in contrast to half-bridge Class-D and full-bridge Class-D, which have 2 and 4 switches, respectively. In the present work, the highest achieved efficiency was 74 % at 1 mm coil distance.

TABLE 7. Comparison to Related Works.

Work	Topology	Frequency	Rating Power	Efficiency @distance	Nº of switches	L_{eq}	Output waveform
[17]	Class-E^{-1}	1000 kHz	14.2 W	84.1 %@8 mm	1	13.96 μH	Sinusoid
[20]	Class-E	1000 kHz	9.87 W	73 %@100 mm	1	23.1 μH	Sinusoid
[26]	Half-Bridge Class-D	98 kHz	48.16 W	85.57 %@100 mm	2	52.7 μH	Sinusoid
[27]	Full-Bridge Class-D	13560 kHz	40 W	91 %@0 mm	4	1.3 μH	Sinusoid
[22]	Class-E	500 kHz	10 W	61 %@30 mm	1	119 μH	Sinusoid
Present	Class-E	500 kHz	9.7 W	74 %@1 mm	1	8.9 μH	Exact

Reference [26] shows a Class-D topology that achieves $85.57\,\%$ efficiency at 100 mm distance. However, it operates at lower frequency, which leads to bigger hardware size as emphasized by the equivalent inductance of$52.7\,\mu$H. The equivalent inductance, i.e., the resonant inductor added to the WPT system equivalent inductor, is reduced in the proposed work. This can be achieved by allowing distortion in the output waveforms, which is predicted by the proposed exact solution. It was shown that the converter maintains ZVS operation over distance variation from tested 1 mm to 7.5 mm. The proposed work contributes to the design of resonant WPT converters by providing the exact solution of the main electrical variables, ultimately, unfolding the theoretical results into hardware design.

AUTHOR'S CONTRIBUTIONS

B.C.NICOLETTI: Data Curation, Formal Analysis, Validation, Visualization, Writing – Original Draft. **F.E.BISOGNO:** Conceptualization, Methodology, Software, Writing – Review & Editing. **L.S.MENDONÇA:** Conceptualization, Data Curation, Formal Analysis, Methodology, Writing – Original Draft.

PLAGIARISM POLICY

This article was submitted to the similarity system provided by Crossref and powered by iThenticate – Similarity Check.

DATA AVAILABILITY

The data used in this research is available in the body of the document.

References

[1] F. T. Carneiro, I. Barbi, "A nálise, Projeto e Implementação de um Conversor com Transferência de Energia Sem Fio para Carregadores de Baterias de Veículos Elétricos", *Eletrônica de Potência - SOBRAEP*, vol. 26, no. 3, pp. 260–267, September 2021, doi:10.18618/REP.2021.3.0003.

[2] R. B. Godoy, E. T. Maddalena, G. de F. Lima, L. F. F. abd V. L. V. Torres, J. O. P. Pinto, "Wireless Charging System With a Non-conventional Compensation Topology for Electric Vehicles and Other Applications", *Eletrônica de Potência - SOBRAEP*, vol. 21, no. 1, pp. 42–51, March 2016, doi:10.18618/REP.2016.1.2575.

[3] D. S. Yeole, A. J. Anil, C. P. Pandit, G. V. Vinayak, "Analysis of Compensation Network in Resonant Inductive Power Transfer (RIPT) for Electric Vehicle Charging", *in 2025 5th International Conference on Trends in Material Science and Inventive Materials (ICTMIM)*, pp. 134–137, 2025, doi:10.1109/ICTMIM65579.2025.10988014.

[4] C. Zhang, N. Tang, W. Zhong, C. K. Lee, R. S. Y. Hui, "A new energy harvesting and wireless power transfer system for Smart Grid", *in 2016 IEEE 7th International Symposium on Power Electronics for Distributed Generation Systems (PEDG)*, pp. 1–5, 2016, doi:10.1109/PEDG.2016.7527006.

[5] J.-Q. Zhu, Y.-L. Ban, Y. Zhang, Z. Yan, R.-M. Xu, C. C. Mi, "Three-Coil Wireless Charging System for Metal-Cover Smartphone Applications", *IEEE Transactions on Power Electronics*, vol. 35, no. 5, pp. 4847–4858, 2020, doi:10.1109/TPEL.2019.2944845.

[6] J. Wu, D. Lan, X. Yu, Y. Zheng, R. Xie, Y. Zhang, "An Inductive and Capacitive Hybrid Wireless Power Transfer System for Consumer Electronics with Shared Components", *in 2024 3rd International Conference on Smart Grids and Energy Systems (SGES)*, pp. 86–89, 2024, doi:10.1109/SGES63808.2024.10824149.

[7] Z. Liang, J. Wang, Y. Zhang, J. Jiang, Z. Yan, C. Mi, "A Compact Spatial Free-Positioning Wireless Charging System for Consumer Electronics Using a Three-Dimensional Transmitting Coil", *Energies*, vol. 12, no. 8, 2019, doi:10.3390/en12081409, URL: https://www.mdpi.com/1996-1073/12/8/1409.

[8] G. L. Barbruni, F. Rodino, P. M. Ros, D. Demarchi, D. Ghezzi, S. Carrara, "A Wearable Real-Time System for Simultaneous Wireless Power and Data Transmission to Cortical Visual Prosthesis", *IEEE Transactions on Biomedical Circuits and Systems*, vol. 18, no. 3, pp. 580–591, 2024, doi:10.1109/TBCAS.2024.3357626.

[9] M. A. de Rooij, "The ZVS voltage-mode class-D amplifier, an eGaN® FET-enabled topology for highly resonant wireless energy transfer", *in 2015 IEEE Applied Power Electronics Conference and Exposition (APEC)*, pp. 1608–1613, 2015, doi:10.1109/APEC.2015.7104562.

[10] M. d. Rooij, "Performance Comparison for A4WP Class-3 Wireless Power Compliance between eGaN FET and MOSFET in a ZVS Class D Amplifier", *in Proceedings of PCIM Europe 2015; International Exhibition and Conference for Power Electronics, Intelligent Motion, Renewable Energy and Energy Management*, pp. 1–8, 2015.

[11] S.-A. El-Hamamsy, "Design of high-efficiency RF Class-D power amplifier", *IEEE Transactions on Power Electronics*, vol. 9, no. 3, pp. 297–308, 1994, doi:10.1109/63.311263.

[12] X. Wei, H. Sekiya, T. Nagashima, M. K. Kazimierczuk, T. Suetsugu, "Steady-State Analysis and Design of Class-D ZVS Inverter at Any Duty Ratio", *IEEE Transactions on Power Electronics*, vol. 31, no. 1, pp. 394–405, 2016, doi:10.1109/TPEL.2015.2400463.

[13] Z. Shu, Y. Fengfa, W. Yijie, J. M. Alonso, "A 500-kHz ZVS Class-E Type DC–DC Converter With Two Anti-Series mosfets Topology", *IEEE Transactions on Power Electronics*, vol. 38, no. 9, pp. 10810–10820, September 2020, doi:10.1109/TPEL.2023.3287161.

[14] M. K. Kazimierczuk, J. Jozwik, "Resonant DC/DC Converter with Class-E Inverter and Class-E Rectifier", *IEEE Transactions on Industrial Electronics*, vol. 36, no. 4, pp. 468–478, November 1989, doi:10.1109/41.43017.

[15] T. Nagashima, X. Wei, E. Bou, E. Alarcón, M. K. Kazimierczuk, H. Sekiya, "Analysis and Design of Loosely Inductive Coupled Wireless Power Transfer System Based on Class-E^2 DC-DC Converter for Efficiency Enhancement", *IEEE Transactions on Circuits and Systems I: Regular Papers*, vol. 62, no. 11, pp. 2781–2791, November 2015, doi:10.1109/TCSI.2015.2482338.

[16] T. Sensui, H. Koizumi, "Load-Independent Class E Zero-Voltage-Switching Parallel Resonant Inverter", *IEEE Transactions on Power Electronics*, vol. 36, no. 11, pp. 12805–12818, 2021, doi:10.1109/TPEL.2021.3077077.

[17] A. Komanaka, W. Zhu, X. Wei, K. Nguyen, H. Sekiya, "Load-Independent Inverse Class-E ZVS Inverter and its Application to Wireless Power Transfer Systems", *IET Power Electronics*, vol. 15, no. 7, pp. 644–658, 2022, doi:10.1049/PEL2.12256.

[18] S. Aldhaher, D. C. Yates, P. D. Mitcheson, "Load-Independent Class E/EF Inverters and Rectifiers for MHz-Switching Applications", *IEEE Transactions on Power Electronics*, vol. 33, no. 10, pp. 8270–8287, 2018, doi:10.1109/TPEL.2018.2813760.

[19] P. Chen, S. He, "Analysis of Inverse Class-E Power Amplifier at Subnominal Condition With 50% Duty Ratio", *IEEE Transactions on Circuits and Systems II: Express Briefs*, vol. 62, no. 4, pp. 342–346, 2015, doi:10.1109/TCSII.2014.2387655.

[20] T. Nagashima, X. Wei, E. Bou, E. Alarcón, H. Sekiya, "Analytical Design for Resonant Inductive Coupling Wireless Power Transfer System with Class-E Inverter and Class-DE Rectifier", *in 2015 IEEE International Symposium on Circuits and Systems (ISCAS)*, pp. 686–689, 2015, doi:10.1109/ISCAS.2015.7168726.

[21] H. Sekiya, X. Wei, T. Nagashima, M. K. Kazimierczuk, "Steady-State Analysis and Design of Class-DE Inverter at Any Duty Ratio", *IEEE Transactions on Power Electronics*, vol. 30, no. 7, pp. 3685–3694, 2015, doi:10.1109/TPEL.2014.2339355.

[22] J. Zhang, J. Zhao, L. Mao, J. Zhao, Z. Jiang, K. Qu, "ZVS Operation of Class-E Inverter Based on Secondary Side Zero Compensation Switching at Variable Coupling Coefficient in WPT", *IEEE Transactions on Industry Applications*, vol. 58, no. 1, pp. 1022–1031, 2022, doi:10.1109/TIA.2021.3125916.

[23] C. Cheng, Y. Zhang, X. Zheng, W. Hua, "A Full-Range Soft-Switching Class-E Inverter Achieving Quasi-Constant Voltage Output", *IEEE Transactions on Power Electronics*, vol. 40, no. 6, pp. 7663–7667, 2025, doi:10.1109/TPEL.2025.3541206.

[24] F. Bennia, A. Boudouda, "Wireless Power Transfer Optimization Using FEM-GA Method", *in 2024 3rd International Conference on Advanced Electrical Engineering (ICAEE)*, pp. 1–6, 2024, doi:10.1109/ICAEE61760.2024.10783287.

[25] M. Jarret, S. Newman, L. Goodman, I. Suzuki, M. Suzuki, "Measurement of mutual inductance from frequency dependence of impedance of AC coupled circuit using digital dual-phase lock-in amplifier", *American Journal of Physics*, vol. 76, 07 2006.

[26] Y. Wang, W. Liu, Y. Huangfu, "A Primary-Sided CLC Compensated Wireless Power Transfer System Based on the Class D Amplifier", *in IECON 2018 - 44th Annual Conference of the IEEE Industrial Electronics Society*, pp. 943–947, 2018, doi:10.1109/IECON.2018.8591707.

[27] H. Tebianian, Y. Salami, B. Jeyasurya, J. E. Quaicoe, "A 13.56-MHz Full-Bridge Class-D ZVS Inverter With Dynamic Dead-Time Control for Wireless Power Transfer Systems", *IEEE Transactions on Industrial Electronics*, vol. 67, no. 2, pp. 1487–1497, 2020, doi:10.1109/TIE.2018.2890505.

BIOGRAPHIES

Bruna Carriel Nicoletti is a mechatronics engineer (2025) with the Federal University of Technology-Paraná. She currently works in software quality. Her areas of interest are: pwm and resonant converters.

Fábio Ecke Bisogno is an electrical engineer (1999), master (2001) in Electrical Engineering with the Federal University of Santa Maria, and doctor in Electrical Engineering with the Technische Universität Chemnitz (2006). He is currently a professor at Hochschule Koblenz. His areas of interest are: resonant converters, self-oscillating electronic converters and artificial lighting.

Lucas Sangoi Mendonça is a control and automation engineer (2015), master (2017) and doctor in Electrical Engineering (2021) with the Federal University of Santa Maria. He is currently a professor at Federal University of Technology-Paraná. His areas of interest are: resonant and pwm dc-dc converters, ac-dc resonant rectifiers and dc-ac resonant inverters.